Three-Dimensional Characteristics of Lightning Channels, Reflectivity Cores, and Vortices in Winter Thunderstorms

Masahide Nishihashi[1,*], Chusei Fujiwara[2], Kenichi Kusunoki[1], Satoru Yoshida[1], Syugo Hayashi[1], Hanako Inoue[1], Ken-ichiro Arai[1], Ken-ichi Shimose[1], Ryohei Kato[1], Sadao Saito[1], Eiichi Sato[1], Wataru Mashiko[1], and Hiroto Suzuki[2]

1. Meteorological Research Institute, Tsukuba, Ibaraki, Japan
2. East Japan Railway Company, Kita-ku, Saitama, Japan

ABSTRACT: A winter thunderstorm was observed in the Shonai area in the northern part of Japan on 30 November 2010. Data from three-dimensional lightning mapping system and two X-band Doppler radars were used to analyze the spatial-temporal relationship between lightning channel, reflectivity core, and airflow structure, especially vortex, in the winter thunderclouds. Lightning leaders propagating from a rim of echo region to the echo region with high reflectivity involving large vertical vorticity were visualized in three dimensions. This result indicates that strong updraft caused by airflow convergence in the precipitation system contributed to accumulate positive charges around -10°C level and enhance vertical vorticity by stretching on the convergence line.

INTRODUCTION

Many studies have documented evidence that lightning activity is associated with severe weather such as wind gusts, tornadoes, and hail (e.g., Goodman et al. 1988; MacGorman et al. 1989; Williams et al. 1989, 1999; Kane 1991; MacGorman and Nielsen 1991; Carey et al. 2003). Recent studies reported that flash rate of total lightning (i.e., both intra-cloud (IC) and cloud-to-ground (CG) lightning) rapidly increases prior to the onset of severe weather events (Williams et al. 1999; Goodman et al. 2005; Steiger et al. 2007; Schultz et al. 2009, 2011; Gatlin and Goodman 2010; Pineda et al. 2011), which Williams et al. (1999) termed "lightning jumps." Gatlin and Goodman (2010) developed an algorithm to identify impending severe weather using the trends in the total flash rate. However, it is difficult to apply the same approach to winter lightning study because winter lightning in the coastal area of the Sea of Japan exhibits various unusual characteristics that have not been observed in the summer in Japan or in any season in other geographical locations (Rakov and Uman 2003).

We have conducted field observations, which we have called "The Shonai Area Railroad Weather Project." The Shonai area is located on the coast of the Sea of Japan. The project was designed in 2007 to investigate the fine-scale structure of wind gusts using two X-band Doppler radars and a network of 26 surface weather stations in order to develop an automatic strong gust (vortex) detection system for

* Contact information: Masahide Nishihashi, Meteorological Research Institute, 1-1 Nagamine, Tsukuba, Ibaraki, Japan, Email: mnishiha@mri-jma.go.jp

railroads (Kusunoki et al. 2008; Inoue et al. 2011). We have focused on total lightning activity in winter to investigate the mechanism of the winter lightning discharge process and the application to the prediction of strong gusts. Thus motivated, we developed a three-dimensional (3D) lightning mapping system for winter thunderstorms using VHF broadband observation (Nishihashi et al. 2013). An observation network for winter lightning was constructed within comprehensive meteorological observation network in the Shonai area. This paper analyzes the spatial-temporal relationship between winter lightning channel, reflectivity core, and airflow structure, especially vortex, in a cold-front thunderstorm on 30 November 2010.

INSTRUMENTATION AND METHODOLOGY

3D Lightning Mapping System

We utilized the 3D lightning mapping system for winter thunderstorms (Nishihashi et al. 2013). To satisfactorily observe lightning discharges over the Shonai area, we arranged a diamond-like sensor array of about 10 km on each side (Fig. 1). During the winter of 2010, there were 4 sites. For continuous remote operation and high-speed data transfer, each site was connected to the Internet through broadband access service (100 Mbps). The VHF lightning observational instrument installed at each station consists of discone antennas, bandpass filters (23–200 MHz), amplifiers (20 dB), a GPS antenna, a GPS receiver, a time generator, a trigger generator, a high-speed digital oscilloscope, and a personal computer (PC). VHF pulses radiated by leader progression were received with three discone antennas arranged in a triangle (antenna distance: 20–30 m) and recorded on the digital oscilloscope (1.25-GHz sampling, 8-bit resolution) with GPS digital timing data (100-ns resolution). The 2D mapping for azimuth and elevation of the VHF radiation sources was conducted by computing the arrival time differences of three pulses using a cross-correlation technique. Azimuth and elevation from two sites for a point source within a given time frame produce 3D lightning image using triangulation scheme.

X-band Doppler radars

We used radar reflectivity data and Doppler velocity data observed with two X-band Doppler radars located at the Shonai airport (MRI radar) and the Amarume station (JR-EAST radar) (Fig. 1). The JR-EAST radar has been operated in a plan position indicator (PPI) mode at one low-elevation angle (3.0°), while the number of elevation angles of the MRI radar was seven for volume scanning. Hence we estimated the wind field at 0.2 km in height inside thunderclouds conducting the dual-Doppler analysis. The spatial resolution of the grid point is 0.2 km.

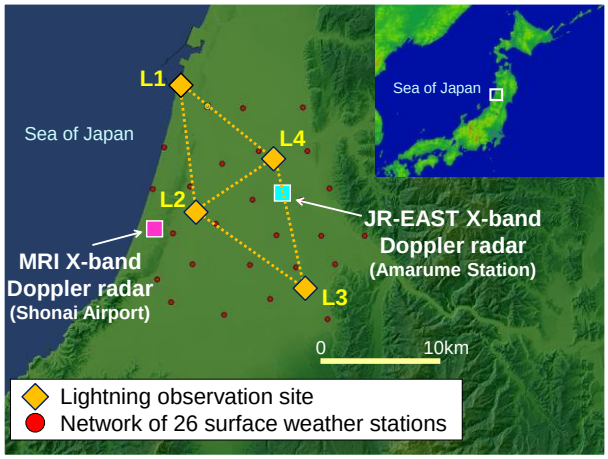

Fig. 1. Location of observation sites. The diamonds indicate the lightning observation sites. The squares denote the X-band Doppler radars and circles indicate the network of 26 surface weather stations.

RESULTS

Figure 2 shows horizontal structure of a narrow cold-frontal rainband observed with the MRI radar and VHF radiation sources from 1321 to 1345 UTC on 30 November 2010. The rainband expanded linearly with a horizontal distance of about 22 km at 1330 UTC. Lightning activity reached a peak from 1330 to 1335 UTC. Figures 3 and 4 show spatial-temporal variation of VHF radiation sources radiated from two lightning flashes at 1332:15 and 1334:38 UTC, respectively. Figures 3 and 4 also show radar reflectivity and Doppler velocity observed at 1330:56 and 1333:21 UTC, respectively. Figure 5 shows radar reflectivity and dual-Doppler synthesized storm-relative horizontal wind vectors at z = 0.2 km for the two flashes. The result of the dual-Doppler analysis shows that the obvious horizontal convergence (> 4×10^{-3} s^{-1}) was formed in the reflectivity core (Fig. 5). Moreover the significant vertical vorticity area (2.5×10^{-2} s^{-1}) is shown on the convergence line. The lightning leaders progressed horizontally from the edge of the radar echo region to the reflectivity core through the echo-top height (10-25 dBZ, around 3 km in altitude) (indicated by red arrows in Figs. 3, 4, and 5). This altitude is consistent with -10°C level (2.9 km) retrieved from Meso-scale Analysis (MANAL) data released by the Japan Meteorological Agency. Figure 6 shows the spatial relationship in 3D between the reflectivity core and the VHF radiation sources. The VHF sources tend to be distributed around isosurface of 25 dBZ.

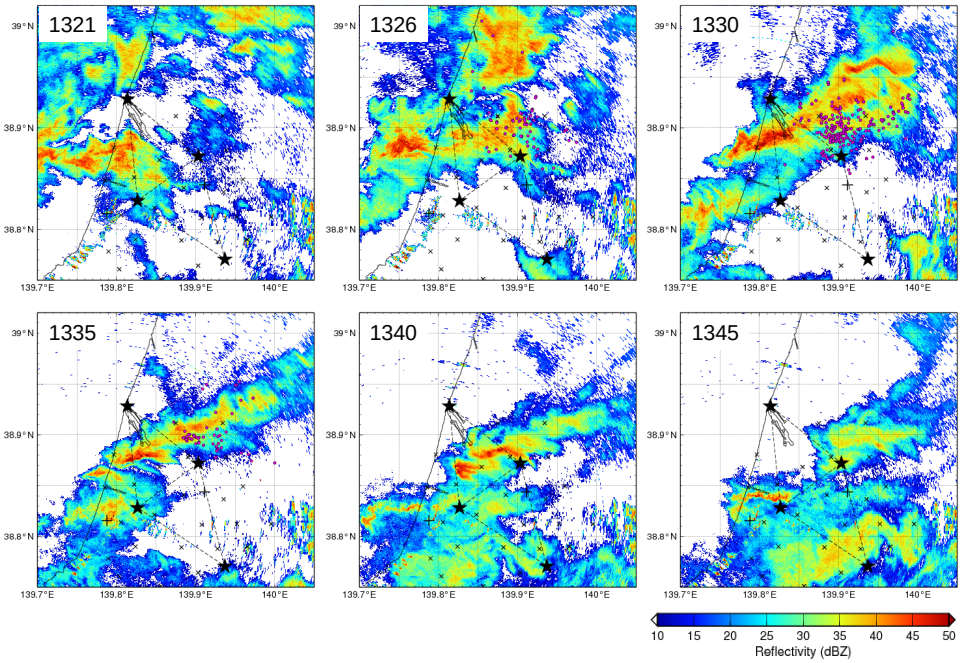

Fig. 2. Evolution of radar reflectivity (PPI scan, elevation angle: 1.8 deg.) observed with the MRI radar and VHF radiation sources (magenta squares) from 1321 to 1345 UTC.

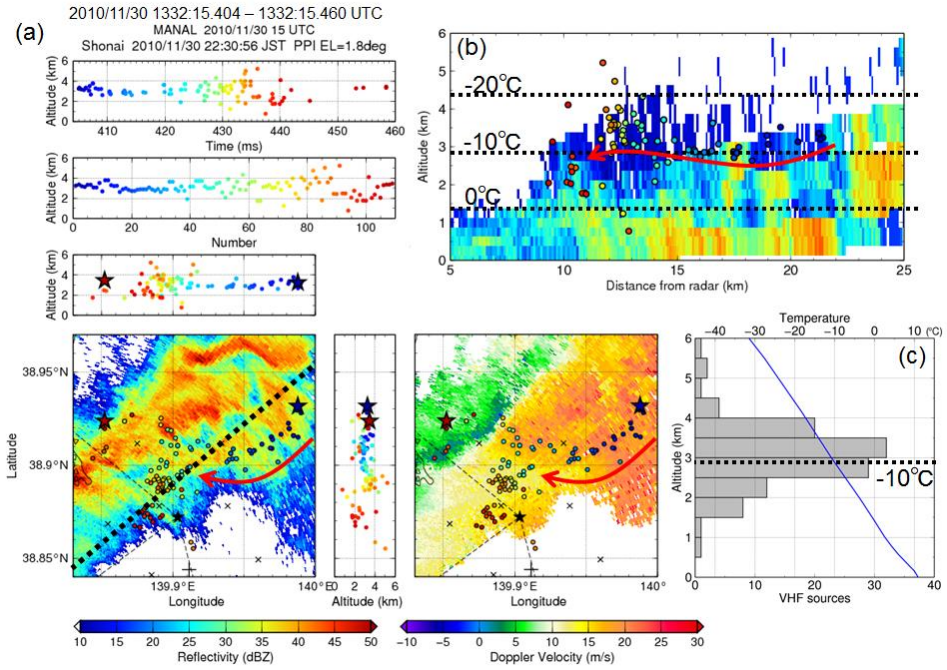

Fig. 3. (a) 3D mapping of VHF radiation sources (1332:15 UTC), radar reflectivity, and Doppler velocity (1330:56 UTC). (b) Vertical cross section of VHF radiation sources and radar reflectivity on the dashed line in (a). (c) Vertical distribution of VHF radiation sources. Blue line indicates temperature profile (1500 UTC) retrieved from MANAL.

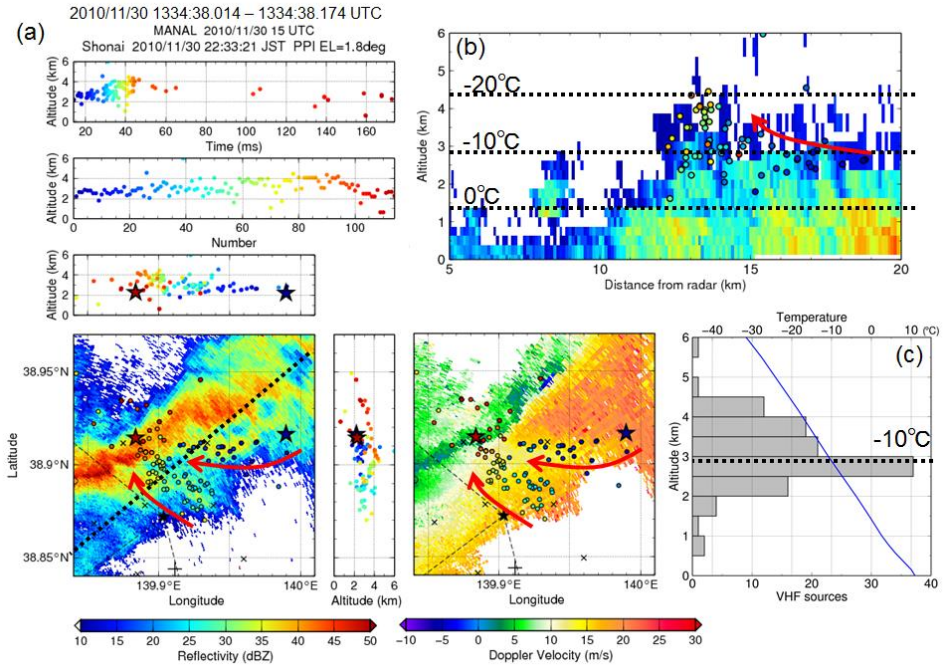

Fig. 4. As in Fig. 3, but lightning flash at 1334:38 UTC and radar data at 1333:21 UTC.

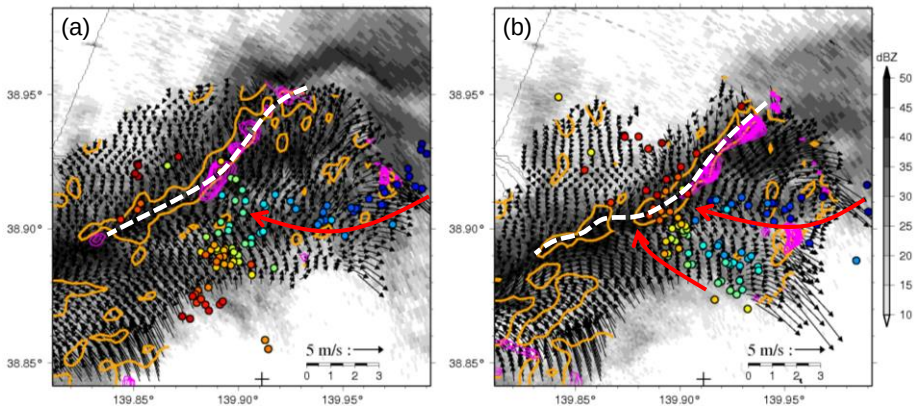

Fig. 5. Radar reflectivity and dual-Doppler synthesized storm-relative horizontal wind vectors at z = 0.2 km for (a) 1330 and (b) 1333 UTC. Orange contours show horizontal convergence (4×10^{-3} s^{-1}). Dashed white line indicates estimated convergence line. Magenta contours denote vertical vorticity every 0.2×10^{-2} s^{-1}, beginning at 1×10^{-2} s^{-1}. Circles represent horizontal distribution of VHF radiation sources at (a) 1332:15 and (b) 1334:38 UTC. Color of the VHF radiation sources indicates time increasing from blue through green to red.

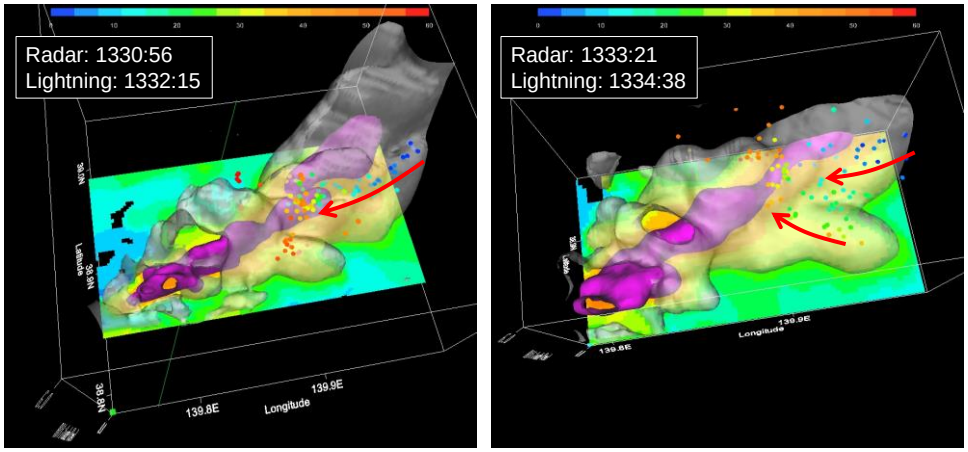

Fig. 6. 3D presentation of 38-dBZ reflectivity isosurface (magenta), 25-dBZ reflectivity isosurface (gray), and VHF radiation sources (circles).

DISCUSSION AND SUMMARY

This is a first result in winter thunderstorm on the coast of the Sea of Japan that the lightning leaders propagating from the rim of the echo region to the reflectivity core involving large vertical vorticity were visualized in 3D. We estimate that the strong updraft caused by airflow convergence in the precipitation system leaded to the following two processes: (1) positive charge accumulation around -10°C level (2.9 km) associated with ice-crystals advection after the charge separation through collisions between graupel and ice crystals caused by the rimming electrification mechanism (Takahashi, 1984), (2) vertical vorticity enhancement by stretching on the convergence line. The result indicates there is a spatial-temporal relationship between lightning discharges and vortex evolutions in winter thunderstorms.

REFERENCES

Carey, L. D., W. A. Petersen, and S. A. Rutledge, 2003: Evolution of Cloud-to-Ground Lightning and Storm Structure in the Spencer, South Dakota, Tornadic Supercell of 30 May 1998. *Mon. Wea. Rev.*, **131**, 1811–1831.

Gatlin, P. N., and S. J. Goodman, 2010: A Total Lightning Trending Algorithm to Identify Severe Thunderstorms. *J. Atmos. Oceanic Technol.*, **27**, 3–22.

Goodman, S. J., D. E. Buechler, P. D. Wright, and W. D. Rust, 1988: Lightning and precipitation history of a microburst-producing storm. *Geophys. Res. Lett.*, **15**, 1185–1188.

Goodman, S. J., R. Blakeslee, H. Christian, W. Koshak, J. Bailey, J. Hall, E. McCaul, D. Buechler, C. Darden, J. Burks, T. Bradshaw, and P. Gatlin, 2005: The North Alabama Lightning Mapping Array: Recent severe storm observations and future prospects. *Atmos. Res.*, **76**, 423–437.

Inoue, H. Y., K. Kusunoki, W. Kato, H. Suzuki, T. Imai, T. Takemi, K. Bessho, M. Nakazato, S. Hoshino, W. Mashiko, S. Hayashi, T. Fukuhara, T. Shibata, H. Yamauchi, and O. Suzuki, 2011: Finescale Doppler Radar Observation of a Tornado and Low-Level Misocyclones within a Winter Storm in the Japan Sea Coastal Region. *Mon. Wea. Rev.*, **139**, 351–369.

Kane, R. J., 1991: Correlating Lightning to Severe Local Storms in the Northeastern United States. *Wea. Forecasting*, **6**, 3–12.

Kusunoki, K., T. Imai, H. Suzuki, T. Takemi, K. Bessho, M. Nakazato, W. Mashiko, S. Hayashi, H. Inoue, T. Fukuhara, T. Shibata, and W. Kato, 2008: An overview of the Shonai area railroad weather project and early outcomes. Preprints, *Fifth European Conf. on Radar in Meteorology and Hydrology*, Helsinki, Finland, European Meteorological Society, P12.1.

MacGorman, D. R., and K. E. Nielsen, 1991: Cloud-to-Ground Lightning in a Tornadic Storm on 8 May 1986. *Mon. Wea. Rev.*, **119**, 1557–1574.

MacGorman, D. R., D. W. Burgess, V. Mazur, W. D. Rust, W. L. Taylor, and B. C. Johnson, 1989: Lightning Rates Relative to Tornadic Storm Evolution on 22 May 1981. *J. Atmos. Sci.*, **46**, 221–251.

Nishihashi, M., K. Shimose, K. Kusunoki, S. Hayashi, K. Arai, H. Y. Inoue, W. Mashiko, M. Kusume, and H. Morishima, 2013: Three-Dimensional VHF Lightning Mapping System for Winter Thunderstorms. *J. Atmos. Oceanic Technol.*, **30**, 325–335.

Pineda, N., J. Bech, T. Rigo, and J. Montanyà, 2011: A Mediterranean nocturnal heavy rainfall and tornadic event. Part II: Total lightning analysis. *Atmos. Res.*, **100**, 638–648.

Rakov, V. A., and M. A. Uman, 2003: *Lightning: Physics and Effects*. Cambridge Univ. Press, 687 pp.

Schultz, C. J., W. A. Petersen, and L. D. Carey, 2009: Preliminary Development and Evaluation of Lightning Jump Algorithms for the Real-Time Detection of Severe Weather. *J. Appl. Meteor. Climatol.*, **48**, 2543–2563.

Schultz, C. J., W. A. Petersen, and L. D. Carey, 2011: Lightning and Severe Weather: A Comparison between Total and Cloud-to-Ground Lightning Trends. *Wea. Forecasting*, **26**, 744–755.

Steiger, S. M., R. E. Orville, and L. D. Carey, 2007: Total Lightning Signatures of Thunderstorm Intensity over North Texas. Part I: Supercells. *Mon. Wea. Rev.*, **135**, 3281–3302.

Takahashi, T., 1984: Thunderstorm Electrification—A Numerical Study. *J. Atmos. Sci.*, **41**, 2541–2558.

Williams, E. R., M. E. Weber, and R. E. Orville, 1989: The Relationship Between Lightning Type and Convective State of Thunderclouds. *J. Geophys. Res.*, **94**, 13213–13220.

Williams, E., B. Boldi, A. Matlin, M. Weber, S. Hodanish, D. Sharp, S. Goodman, R. Raghavan, and D. Buechler, 1999: The behavior of total lightning activity in severe Florida thunderstorms. *Atmos. Res.*, **51**, 245–265.